View Article Online / Journal Homepage / Table of Contents for this issue
Dynamic Article Links

PCCP

Cite this: *Phys. Chem. Chem. Phys.*, 2011, **13**, 20729–20735

www.rsc.org/pccp

PAPER

Published on 14 October 2011. Downloaded by Technische Universitat Braunschweig on 18/02/2016 07:55:42.

Neutron diffraction study of water freezing on aircraft engine combustor soot

V. Tishkova,†*[a] B. Demirdjian,[a] D. Ferry[a] and M. Johnson[b]

Received 8th April 2011, Accepted 19th September 2011
DOI: 10.1039/c1cp21109a

The study of the formation of condensation trails and cirrus clouds on aircraft emitted soot particles is important because of its possible effects on climate. In the present work we studied the freezing of water on aircraft engine combustor (AEC) soot particles under conditions of pressure and temperature similar to the upper troposphere. The microstructure of the AEC soot was found to be heterogeneous containing both primary particles of soot and metallic impurities (Fe, Cu, and Al). We also observed various surface functional groups such as oxygen-containing groups, including sulfate ions, that can act as active sites for water adsorption. Here we studied the formation of ice on the AEC soot particles by using neutron diffraction. We found that for low amount of adsorbed water, cooling even up to 215 K did not lead to the formation of hexagonal ice. Whereas, larger amount of adsorbed water led to the coexistence of liquid water (or amorphous ice) and hexagonal ice (I_h); 60% of the adsorbed water was in the form of ice I_h at 255 K. Annealing of the system led to the improvement of the crystal quality of hexagonal ice crystals as demonstrated from neutron diffraction.

Introduction

Aircraft particulate emissions into the atmosphere induce condensation trails (contrails)[1] and cirrus clouds formation,[2,3] which may modify the radiative balance of the atmosphere and have an effect on the climate.[4,5] Line-shaped condensation trails can grow to contrail-cirrus clouds and cover nine times higher surface than young contrails.[6] Radiative forcing caused by contrail induced cloudiness is one of the largest aviation-related radiative-forcing components.[6] Homogeneous freezing of solution droplets and heterogeneous nucleations on ambient particles are involved in cloud formation processes, and the domination of one of these mechanisms can change the albedo of a cloud.[6] An experimental study of residual nuclei in cirrus clouds shows the presence of solid particles which are involved in heterogeneous nucleation, and the presence of soluble (sulfates and salts) particles, which freeze homogeneously at the altitude of aircraft traffic.[7] Carbonaceous particles (soot) emitted by aircraft engines have been found in condensation trails[8] where they can act as nuclei for heterogeneous nucleation.[9] Typically hexagonal ice is formed, but metastable cubic ice formation is also observed in conditions relevant to the stratosphere and upper troposphere.[10–12]

In this work, we focused on the investigation of the ice formation on soot particles emitted from an aircraft engine combustor chamber in order to evaluate the role of these soot particles on contrail and cirrus cloud formation.

The mechanism of water/soot interaction is related to the ability of soot particles to act as cloud condensation nuclei (CCN) and ice nuclei (IN). Soot particles can be classified as hydrophobic, hydrophilic or hygroscopic based on the amount of adsorbed water.[13] Aircraft engine combustor (AEC) soot is found to be extremely hygroscopic since the amount of adsorbed water is much higher than the one found for commercial and laboratory produced samples.[13] Water/soot interaction in the case of AEC soot particles is more complicated because of the presence of a relatively high water soluble fraction (WSF) and surface functional groups forming strong hydrogen bonds.[13,14] Several investigations[15–20] show that the WSF together with the surface chemistry are important parameters for CCN and IN activities of soot particles. Ozone treatment[20] suppresses the ice nucleation ability of pure soot particles. And another study show that coating of soot particles with sulfuric acid can also change the ice nucleation threshold.[17,19] Neutron diffraction (ND) and quasi-elastic neutron scattering (QENS) studies of water freezing on laboratory produced kerosene flame soot (KFS)[21,22] show that KFS is a potential candidate for ice nucleation in atmosphere. Moreover, it has been observed that sulfuric acid activation facilitates the formation of hexagonal ice which is stable till 210 K.

Experimental study of the nucleation of ice crystals on original aircraft engine combustor (AEC) soot is needed to evaluate effects of the aircraft particulate emission on the extra

[a] *CINaM‡/UPR CNRS 3118, Campus de Luminy, 13288 Marseille Cedex 9, France. E-mail: victoria.tishkova@cemes.fr*
[b] *Institut Laue-Langevin, BP 156, 6 rue Jules Horowitz, 38042 Grenoble Cedex 9, France*
† Current address: CEMES/CNRS, 29 rue Jeanne Marvig BP 94347, 31055, Toulouse Cedex 4, France.
‡ Associated to Aix-Marseille University.

View Article Online

Published on 14 October 2011. Downloaded by Technische Universitat Braunschweig on 18/02/2016 07:55:42.

cloudiness and their role in general as active cloud condensation nuclei (CCN) and ice nuclei (IN) in the atmosphere.

In this work, first, we described the physico-chemical properties of AEC soot particles as microstructure, elemental composition, surface chemistry and water interaction. Then we reported the novel neutron diffraction (ND) studies on the ice formation on AEC soot.

Experiment

Soot sample and its physico-chemical characterization

Aircraft Engine Combustor (AEC) soot was collected at the outlet of a combustor chamber on a dedicated facility. Aviation kerosene TC1 was used as fuel and the sampling was performed at a minimum distance of 12 cm of the chamber exit in order to avoid the influence of the reactive gases. A relatively large amount of sample is needed in order to perform ND experiments and obtain a good signal-to-noise ratio when only a few water monolayers are adsorbed on the sample. Hence a total mass of 1.4 g was collected at the end of several runs. A detailed description of the sampling procedure is presented elsewhere.[23] Kerosene flame soot (KFS) was produced by burning the same aviation kerosene TC1 but in a wick oil lamp and was used as a reference (see ref. 23 for more details).

A transmission electron microscope (TEM) JEOL 2000 FX (200 keV) with a spatial resolution of 2.8 Å was used to investigate the microstructure of the sample. The crystallinity and elemental composition were determined by selected area electron diffraction (SAED) and energy dispersive spectroscopy (EDS, TRACOR series II) coupled to the TEM, respectively. Samples were directly deposited on a Cu microgrid coated with an amorphous C-holey film without solvent to avoid contamination of the soot particles. Surface chemistry was investigated using Infrared spectroscopy (Fourier Transform InfraRed (FTIR) spectrometer (Bruker Equinox 55) in standard transmission configuration). The soot sample was placed on a germanium window by pressing the powder, without any solvent. Spectra were recorded in the range from 400 to 4000 cm^{-1} with a resolution of 4 cm^{-1} and averaged over 400 scans. The spectrometer was continuously purged with dry air in order to eliminate signals from carbon dioxide and water vapor.

Neutron diffraction measurements

Both Neutron Diffraction (ND) and electron microscopy measurements were used to have a complete picture of the microstructure of AEC soot. ND experiments were performed on a high-intensity two-axis diffractometer D20 (Institute Laue-Langevin (ILL), Grenoble, France). A wavelength of 2.41 Å was used. Diffraction patterns were recorded using a one-dimensional position-sensitive detector which covers a scattering angle range of 153.6°. A more detailed description of the D20 diffractometer is given in ref. 24.

D_2O was used instead of H_2O in order to achieve a good signal-to-background ratio. The soot sample was placed in a vanadium cell and was pumped gradually to a pressure $P < 10^{-2}$ torr prior to the experiments. The sample temperature was varied from 280–180 K using a cryostat. A desired amount of water can be introduced in the cell through a calibrated volumetric system where water pressure is controlled and measured. The water vapor pressure was controlled by a gauge MKS BARATRON 100 torr with an accuracy of 0.25% on the reading. We were waiting until the pressure was stable at all investigated temperatures. Relative humidity is calculated as $RH = \frac{P}{P_s} \times 100\%$ where P is the partial pressure of water vapor and P_s is the saturated vapor pressure at a given temperature. The experimental protocol is presented in Fig. 1. Initially, an amount of water corresponding to 4 statistical monolayers (ML) was introduced into the system at 280 K, then the sample was cooled down to record spectra at 260 K, 235 K and 215 K. Following this, the temperature was increased to 280 K and 4 more ML of water were introduced , the sample was then cooled again to 255 K, 235 K, 215 K and 180 K. ND spectra were recorded at each mentioned temperature. The effect of the annealing was investigated by heating up the sample to 280 K and cooling it again to 255 K. No additional water was introduced at this step. The collection time was 4 h for all the spectra so that a good signal/noise ratio was obtained. The background spectra corresponding to bare soot were recorded at 280 K and 260 K prior to water adsorption on the sample, they allow us to determine the water/ice signal by subtracting them to the (soot + water/ice) spectra.

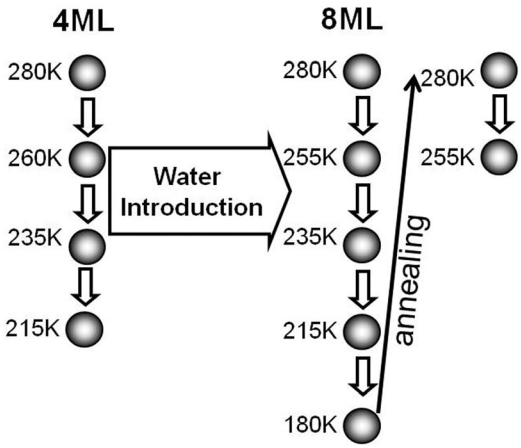

Fig. 1 Routine of the ND experiments at ILL (Grenoble) on the diffractometer D20. Water is introduced at 280 K.

ND spectra for KFS were recorded on the two-axis powder diffractometer G4-1 (Laboratory Leon Brillouin (LLB) Saclay, France). This diffractometer was equipped with a vertical focusing pyrolytic graphite monochromator and a 800-cells multidetector covering a 80°—2θ range (step 0.1° between two cells). We used a neutron beam with a wavelength of 2.42 Å. The sample was placed in the same vanadium cell and we used the same volumetric calibrated system to introduce water in the cell. More details on the water freezing experiments on KFS are found in ref. 22.

Results and discussions

Microstructure

ND spectra of AEC soot and KFS are presented in Fig. 2, they are similar to those observed for turbostratic or carbon

 This journal is © the Owner Societies 2011

View Article Online

Published on 14 October 2011. Downloaded by Technische Universitat Braunschweig on 18/02/2016 07:55:42.

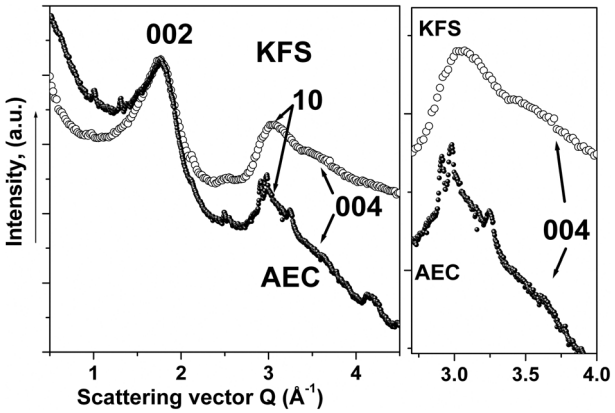

Fig. 2 ND spectra of kerosene flame soot (KFS) and aircraft engine combustor soot (AEC). Zoom on the peak 10 and the shoulder 004 are presented on the right graphic.

black structure.[26] We observed a broad (002) peak that corresponds to graphene interplane distances in the graphite microcrystallites and a peak (10) with a shoulder corresponding to the (004) reflection (see zoom in Fig. 2). Lattice parameters (Table 1) were found to be in good agreement with the one found in the literature for commercial carbon blacks.[26,27] The Scherrer equation was used to calculate the crystallite sizes.[28] It was found that the size L_c along the [002] crystallographic direction of AEC and KFS soot microcrystallites was about the same whereas the size L_a along the [10] direction was larger for AEC soot microcrystallites than for the KFS ones (Table 1). We also found that AEC and KFS soot microcrystallites were made of 3 and 4 graphene layers in average, respectively.

The AEC spectrum (Fig. 2) exhibits diffraction peaks of carbon black and some additional components that are not visible in the KFS spectrum. TEM and EDS analysis show that AEC soot had a heterogeneous microstructure and was composed of two fractions. The main fraction was made of primary soot-type particles with a mean diameter of 35–50 nm. The elemental composition of this fraction was homogeneous and is mainly composed of carbon, oxygen and sulfur. The other fraction of impurities was mainly made of iron oxides, sulfur, copper, zinc and aluminium. A typical TEM image showing the coexistence of the main fraction (spherical particles) and the fraction of impurities (iron oxide rods) is presented in Fig. 3. SAED was measured on the impurities (dark rods) and it is shown in the inset in Fig. 3. It proves the presence of fine nanocrystals that are oriented at different angles with respect to the electron beam. The measurement of interplanar distances, associated with an EDS study, showed the presence

Table 1 Lattice parameters, mean microcrystallites size, and the mean number of graphene planes in a graphite microcrystallite determined from ND spectra for KFS and AEC soot samples

Sample	Lattice parameters/Å	Microcrystallites size/Å	Mean number of graphene planes
KFS	$d_{002} = 3.58 \pm 0.20$	$L_a = 13 \pm 2$	4
	$d_{10} = 2.05 \pm 0.10$	$L_c = 13 \pm 2$	
AEC	$d_{002} = 3.58 \pm 0.20$	$L_a = 21 \pm 2$	3
	$d_{10} = 2.07 \pm 0.10$	$L_c = 10 \pm 1$	

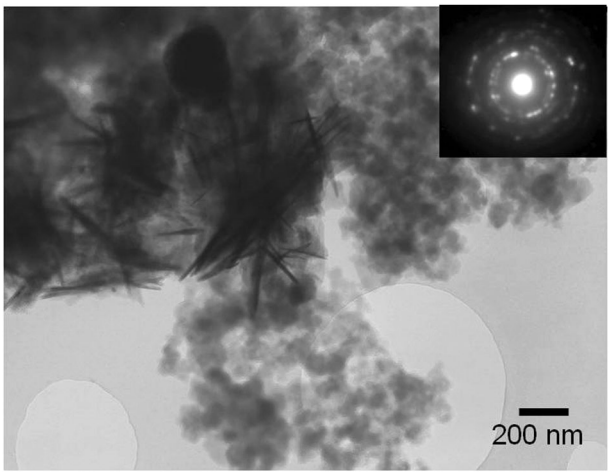

Fig. 3 TEM image of the main fraction (spherical soot particles) and the fraction of impurities (dark rods) of AEC soot. Inset: SAED pattern obtained on the impurities.

of iron and oxygen in the selected area. It leads us to the conclusion that these rods correspond to iron oxide (FeO) crystals. It is further confirmed from the ND peaks that show the presence of particles containing iron (FeO, FeO(OH)), copper (CuO, Cu_2O) and aluminium ($Al(OH)_3$).[29] The source of these impurities could be the result of ageing of the combustor chamber and its parts. However, due to the overlap of the graphite and the various metal oxide peaks in the ND, the exact quantities of each fraction cannot be determined.

TEM and EDS studies of KFS show that it mainly consists of roughly spherical, carbon particles formed by microcrystallites of graphite arranged in the form of a turbostratic structure. The KFS sample can be used only as a surrogate to the main fraction of the AEC soot.[23]

Surface chemistry

FTIR spectra of KFS and AEC soot samples are presented in Fig. 4. These spectra exhibit the typical underlying absorption of a carbon skeleton[30] (–C–C– and –C=C–) in the range 800–1600 cm^{-1}. The out-of-plane C–H vibrations in polyaromatic

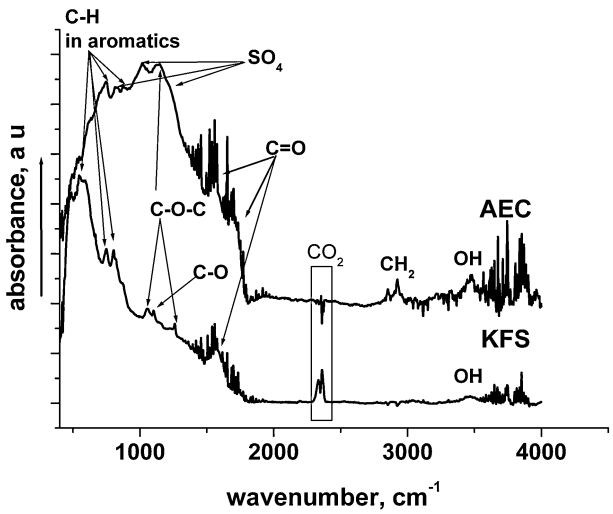

Fig. 4 FTIR spectra of KFS and AEC soots at room temperature.

View Article Online

Published on 14 October 2011. Downloaded by Technische Universitat Braunschweig on 18/02/2016 07:55:42.

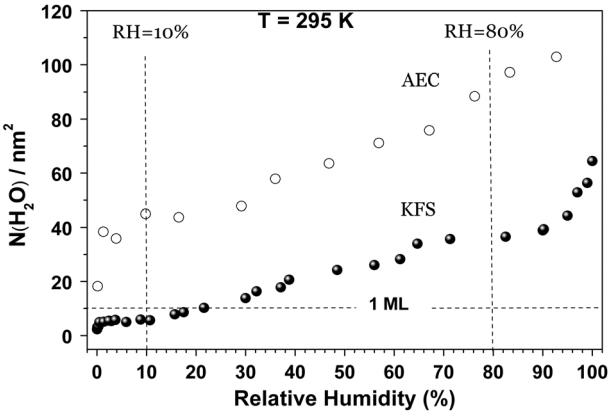

Fig. 5 Water adsorption isotherms on KFS and AEC soot samples at room temperature[11] (T = 296 K).

compounds were observed in the region 700–900 cm^{-1} for both samples.[31] Oxygen containing functional groups such as asymmetric C–O–C vibrations and C=O in carboxylic acid or quinone[32] were also detected for both samples (KFS: 1100 cm^{-1}, 1260 cm^{-1}, and 1580 cm^{-1}; AEC: 1124 cm^{-1}, 1150 cm^{-1}, 1560 cm^{-1}, and 1700 cm^{-1}). Absorption peaks for AEC soot were observed at 2850 cm^{-1} and 2925 cm^{-1}, which correspond to the symmetric and asymmetric vibrations of CH_2, respectively. The peak detected at 3470 cm^{-1} is a result from OH vibrations, and is present in both spectra of AEC and KFS soot. Other peaks corresponding to 810 cm^{-1}, 1050 cm^{-1}, and the shoulder at 1220 cm^{-1} were only observed for AEC soot and relate to the sulfate ion SO_4^{2-} vibrations.[30,32] This result is in good agreement with ion chromatography studies[15] that show up to 3.5 wt% of ionic sulfates extracted from AEC soot. On the other hand, KFS has a smaller water soluble fraction (~0.3 wt%), and a negligible amount of sulfate ions ($<1.5 \times 10^{-3}$ g cm^{-3}).[14] Thus, we exclude the presence of any sulfates on the KFS soot surface.

Water freezing

In our previous study we investigated water adsorption on AEC soot at the room temperature.[13] Isotherms of water adsorption on KFS and AEC samples at room temperature are presented in Fig. 5. Carrot[33] has proposed to use one statistical monolayer (ML) to characterize the polarity of the soot samples. Indeed, water adsorption on soot particles takes place on active sites and then forms clusters[34] which is described by classical theory of water adsorption.[13] Here, we calculated one statistical monolayer assuming an effective water molecular area is 0.105 nm^2.[33] The total amount of adsorbed water on AEC soot is much higher than that on KFS. Based on the amount of adsorbed water, AEC soot has been classified as hygroscopic soot,[13] whereas KFS has been classified as hydrophobic soot.[13,23] KFS is proposed as a surrogate for the hydrophobic fraction of the AEC soot. The high amount of water uptake on AEC soot compared to KFS and the high water soluble fraction led us to the conclusion that the mechanism of AEC water/soot interaction is not described by the classical theory.[13] The principal mechanism of water–AEC soot interaction is dissolution of the water soluble fraction (WSF).[13]

Here, we study water freezing of 4 and 8 statistical ML that were adsorbed on AEC soot at room temperature. These amounts of adsorbed water correspond to relative humidities (RH) of 10% and 80%, respectively (Fig. 5). Investigation of the water adsorption on AEC soot at temperatures down to 233 K shows that the amount of adsorbed water at high RH increases as the temperature decreases.[35] We assume that 4 ML of water molecules do not form a bulk structure even at low temperature as no signature of the ice I_h phase was measured by neutron diffraction. Diffractograms corresponding to the cooling of 4 ML of water adsorbed on AEC soot show a broad asymmetric peak at 1.86 $Å^{-1}$ (noncrystalline structure), which is observed even at 215 K (Fig. 6). This broad peak can be assigned to liquid water confined in micropores and/or low density amorphous ice.[22,36]

Diffractograms corresponding to the cooling and warming cycles of 8 ML of water adsorbed on AEC soot are shown in Fig. 7. One can observe the broad peak that is present for 4 ML, and sharp peaks detected at temperatures lower than 255 K. These sharp peaks correspond to the (100), (002), (101), (102), (110), and (103) reflections of the hexagonal ice I_h structure (Fig. 7). However, cubic ice I_c also exhibits

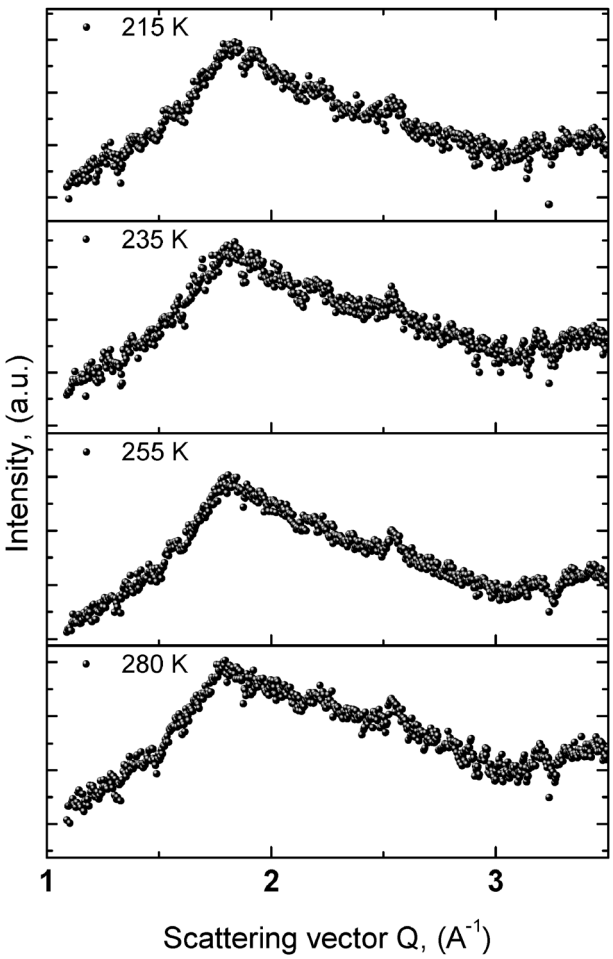

Fig. 6 Neutron diffraction spectra of 4 ML of water adsorbed on AEC soot at different temperatures 280 K, 260 K, 235 K, and 215 K (background spectra are subtracted). No ice formation is observed down to 215 K.

 This journal is © the Owner Societies 2011

View Article Online

Published on 14 October 2011. Downloaded by Technische Universitat Braunschweig on 18/02/2016 07:55:42.

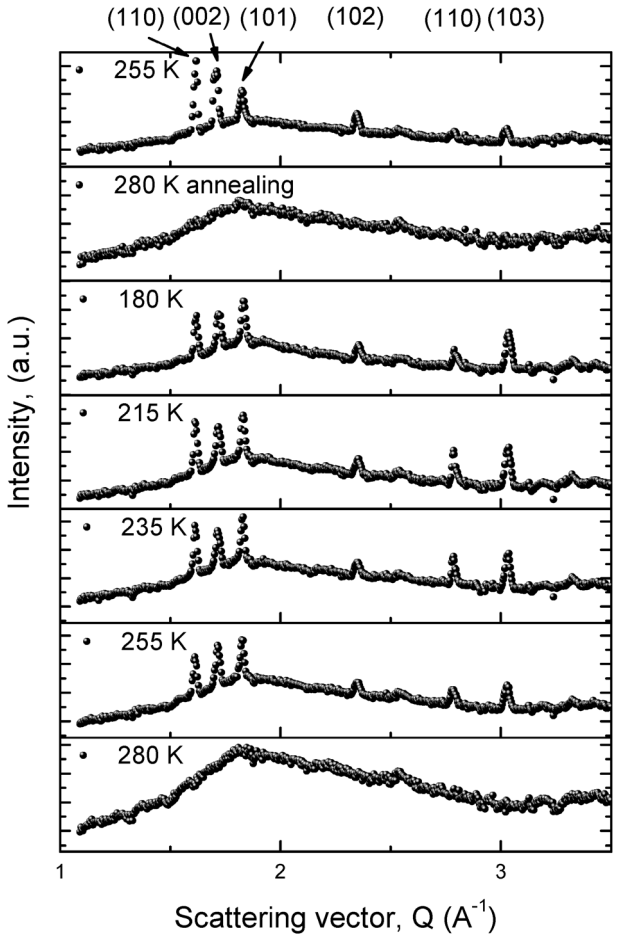

Fig. 7 Neutron diffraction spectra of 8 ML of water adsorbed on AEC soot at different temperatures and effect of the annealing at 280 K.

reflections at the same position than some of ice I_h reflections. Indeed, the (111) and (220) reflections of ice I_c structure are located at the positions of the (002) and (110) peaks of ice I_h,[37] respectively. It is then not possible to determine if ice I_c is formed from ND spectra because of the overlapping of several ice I_h and ice I_c reflections.

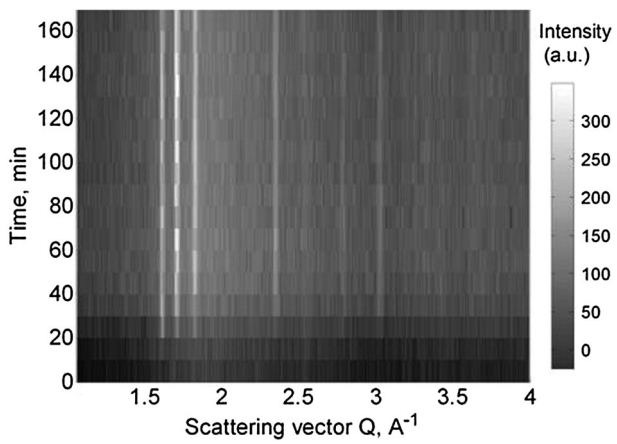

Fig. 8 Ice growth on AEC soot at 255 K (8 ML) *vs.* time (the lighter parts correspond to the higher intensities); the formation of the triplet of hexagonal ice is seen after 20 minutes.

We also investigated the kinetics of ice formation with time at 255 K. The ND spectra were recorded during 180 minutes with a time step of 10 minutes. As it is shown in Fig. 8, peaks of I_h appeared in 20 minutes of recording and the intensity remains constant. We conclude therefore that the ice I_h was formed after 20 minutes.

The results obtained for the freezing of 4 ML of water are surprising since we found that water remains liquid/amorphous and didn't form crystalline ice, even at low temperature (215 K). However, supercooled water has already been observed in porous systems,[38] but the pore volume of AEC soot is low,[35] even lower than that of commercial and laboratory made samples. This low porosity can be explained by a high fraction of soluble and volatile components on the surface, which can fill or close the pores. Laboratory studies showed that organic carbon coating of soot particles decreases the fraction of ice on soot particles.[18] If organic carbon is present in the WSF, it may influence the water freezing. On the other hand, the presence of sulfate ions in WSF could explain that water does not freeze at 215 K in AEC soot samples. It has been shown[39–41] that H_2SO_4/water droplets with a concentration more than 35 wt% are difficult to freeze homogeneously, even at 190 K. Other experiments on heterogeneous freezing of sulfuric acid droplets with a concentration of 5–20 wt% in the presence of graphite particles have shown an upshift of the freezing temperatures, compared to homogeneous freezing, by about 10 K.[42] Coating of soot particles with sulfuric acid increases the saturated vapor pressure needed to nucleate ice compared to pure soot particles and the saturation needed for the ice nucleation is close to the one needed for homogeneous nucleation of sulfuric acid droplets.[17] As already mentioned,[13] the main mechanism of the interaction of water molecules with hygroscopic AEC soot particles is the dissolution of the water soluble fraction. A mixture of water and sulfuric acid may be formed, and a further addition of water molecules will lower the sulfuric acid concentration, and thus favor the formation of crystalline ice. However, the coexistence of the broad peak located at 1.86 $Å^{-1}$ with sharp peaks of crystalline ice I_h means that a liquid phase (or an amorphous solid phase) and the ice I_h solid phase were present even at 180 K and remained also visible after annealing. Similar results, showing that around 30% of water is transformed to ice on KFS soot at $T = 240$ K, have been obtained by quasi-elastic neutron scattering (QENS). The fraction of liquid water decreases with temperature, so that at 200 K only 15% of water molecules remain in the liquid phase.[21,22] In order to quantify the fraction of ordered (ice I_h) and disordered (liquid and/or amorphous) water phases at different temperatures, we compared the ratio of the surface areas of the large peak (disordered phase) and sharp peaks of ice. Note that quantitative results from QENS and ND need to be compared with caution since QENS measures the mobility of water molecules, whereas ND allows determining the crystallinity. The disordered fraction can be either liquid or amorphous solid water, but QENS enables to distinguish between the amorphous liquid and solid phases in contrast to ND. We observed an increase of the ice I_h fraction with a temperature decrease, leading to a value of about 60% of water molecules in this ordered solid phase at 180 K. In the case of

View Article Online

Published on 14 October 2011. Downloaded by Technische Universitat Braunschweig on 18/02/2016 07:55:42.

Table 2 Size of the ice microcrystallites determined from the Scherrer equation

	Microcrystallites size (Å) at different temperatures				
hkl	255 K	235 K	215 K	180 K	255 K (annealing)
100	570	936	694	650	1145
002	380	341	333	328	342
101	1000	1150	639	451	349
102	247	185	149	228	194
110	233	504	452	142	50
103	468	234	175	345	102

KFS, 40% of water was solid at 220 K, but treating the KFS surface with sulfuric acid led to an increase of the frozen part from 40% to 70%.[22]

An annealing of the system up to 280 K followed by a cooling down to 255 K led to a better structured ice. This latter point was evidenced by an increase of the relative intensities of the ice I_h reflections.[43] The hexagonal ice I_h fraction at 255 K also increases from 40% to 55% before and after annealing, respectively. The size of ice I_h microcrystallites along various crystallographic directions was determined from the Scherrer equation[28] and values are presented in Table 2. We note that the size of the ice microcrystallites increased in the [100] direction during the annealing, whereas it remained constant in the [002] direction during the freezing and annealing.

In summary, we observe that ice was not formed at low content of adsorbed water, whereas it coexisted with liquid or amorphous solid water at higher water content (close to saturation). Surface chemistry of soot particles and specific water–soot interaction are likely to play an important role in ice nucleation processes promoted by these soot particles.[22] However, the presence of a relatively high WSF is not favorable for ice nucleation. Our results agree with previous investigations of ice nucleation on AEC soot. Indeed, although it has been shown that conditions needed to form ice on AEC soot are close to those for homogeneous freezing,[15] experimental results obtained by Cziczo *et al.*[44] also show that coating of dust particles with sulfuric acid decreases the ability to nucleate ice.

Conclusion

The present work is focused to study the soot microstructure and the ice formation on aircraft engine combustor (AEC) soot. We showed that the AEC has heterogeneous microstructure. It contains primary soot particles, which are typical of carbon blacks, and metallic impurities (FeO, FeO(OH), CuO, Cu_2O and $Al(OH)_3$). In contrast to AEC soot, laboratory made soots like KFS do not contain any metallic impurities. Based on our ND measurements, we determined the lattice parameters and the size of soot microcrystallites that compose both AEC and KFS samples. We found that the lattice parameters were close to the ones of turbostratic graphite, in agreement with previously observed values for soot particles.[25] We also found that AEC and KFS soot microcrystallites had the same size in the [002] crystallographic direction, whereas AEC microcrystallites were larger than KFS ones in the [10] direction.

Water–soot interaction is important for understanding the fate and impact of the aircraft carbonaceous emission in the atmosphere. Indeed, soot particles can act as ice nuclei to form cirrus clouds and contrails. The knowledge of surface functional groups and water soluble fraction is important as they may play a role in the water–soot interactions.[13] Various surface functional groups including oxygen-containing functional groups are observed for KFS and AEC soot. However, sulfate ions are only observed in AEC soot samples. The water uptake on AEC soot is relatively high compared to laboratory-made and commercial soot samples.[13] We showed in ND experiments that at low temperature and a relatively small amount of adsorbed water, corresponding to 4 ML and low RH, there was no signature of cubic neither hexagonal ice phase on the spectra. But there was only a signal that can be related to a liquid water phase or a low density amorphous ice phase. At a higher amount of adsorbed water, 8 ML, we observed the formation of hexagonal ice below 255 K that coexisted with a liquid and/or amorphous ice phase till 180 K. An annealing led to the formation of a better ordered hexagonal ice structure, but the broad peak of liquid-like water remained visible on ND spectra. This result may be explained by the relatively high WSF containing sulfate ions. We assume that when water molecules are adsorbed, the WSF may contain sulfuric acid that limits the process of freezing even at the lowest temperatures. Our results showed that AEC soot particles can act as ice nuclei to form condensation trails at high relative humidity, but its impact on the cirrus clouds should be investigated together with the effect of the AEC soot aging and evolution of its hygroscopic properties.

Acknowledgements

The authors acknowledge the I.L.L. and the L.L.B. for access to the neutron facilities and T. Hansen (I.L.L.) and G. Andre (L.L.B.) for their help with the measurements. The authors also thank O. Popovicheva for providing the soot samples.

References

1 B. Kärcher and F. Yu, *Geophys. Res. Lett.*, 2009, **36**, L01804.
2 O. Boucher, *Nature*, 1999, **397**, 30–31.
3 J. Hendricks, B. Kärcher, U. Lohmann and M. Ponateri, *Geophys. Res. Lett.*, 2005, **32**, L12814.
4 J. Haywood and J. Boucher, *Rev. Geophys.*, 2000, **4**(38), 513–543.
5 D. C. Lee, G. Pitari, V. Grewe, K. Gierens, J. E. Penner, A. Petzold, M. J. Prather, U. Schumann, A. Bais, T. Berntsen, D. Lachetti, L. L. Lim and R. Sausen, *Atmos. Environ.*, 2010, **44**, 4678–4734.
6 U. Burkhardt and B. Kärcher, *Nat. Clim. Change*, 2011, **1**, 54–58.
7 C. H. Twohy and M. R. Poellot, *Atmos. Chem. Phys.*, 2005, **5**, 2289–2297.
8 A. Petzold, J. Strom, S. Ohlsson and P. I. Schroder, *Atmos. Res.*, 1998, **49**, 21–34.
9 A. P. Fornea, S. D. Brooks, J. B. Dooley and A. Saha, *J. Geophys. Res.*, 2009, **14**, D13201.
10 B. J. Murray, D. A. Knopf and A. K. Bertram, *Nature*, 2005, **434**, 202–204.
11 B. J. Murray, *Environ. Res. Lett.*, 2008, **3**, 025008.
12 D. M. Murphy, *Geophys. Res. Lett.*, 2003, **30**(23), 2230.
13 O. B. Popovicheva, N. M. Persiantseva, V. V. Tishkova, N. K. Shonija and N. A. Zubareva, *Environ. Res. Lett.*, 2008, **3**, 025009.
14 O. B. Popovicheva, N. M. Persiantseva, E. Lukhovitskaya, B. Demirdjian, D. Ferry and J. Suzanne, *Geophys. Res. Lett.*, 2004, **31**, L11104.

 This journal is © the Owner Societies 2011

View Article Online

Published on 14 October 2011. Downloaded by Technische Universitat Braunschweig on 18/02/2016 07:55:42.

15 K. A. Koehler, P. J. DeMott, S. M. Kreidenweis, O. B. Popovicheva, M. D. Petters, C. M. Marrico, E. D. Kireeva, T. D. Khokhlova and N. K. Shonija, *Phys. Chem. Chem. Phys.*, 2009, **11**, 7906–7920.
16 G. Lammel and T. Novakov, *Atmos. Environ.*, 1995, **29**, 813–823.
17 O. Möhler, S. Buttner, C. Linke, M. Schnaiter, H. Saathoff, O. Stetzer, R. Wagner, M. Kramer, A. Mangold, V. Ebert and U. Schurath, *J. Geophys. Res.*, 2005, **110**, D11210.
18 O. Möhler, C. Linke, H. Saathoff, M. Schnaiter, R. Wagner, A. Mangold, M. Krämer and U. Schurath, *Meteorol. Z.*, 2005, **14**(4), 477–484.
19 D. J. Demotte, Y. Chen, S. M. Kreidenweis, D. C. Rogers and D. E. Sherman, *Geophys. Res. Lett.*, 1999, **26**(16), 2429–2432.
20 M. Dymarska, B. J. Murray, L. Sun, M. L. Eastwood, D. A. Knopf and A. K. Bertram, *J. Geophys. Res.*, 2006, **111**, D04204.
21 J. Suzanne, D. Ferry, O. B. Popovicheva and N. K. Shonija, *Can. J. Phys.*, 2003, **81**, 423–429.
22 B. Demirdjian, D. Ferry, J. Suzanne, O. Popovicheva, N. M. Persiantseva, A. V. Kamaev, N. K. Shonija and N. A. Zubareva, *Chem. Phys. Lett.*, 2009, **480**(4–6), 247–252.
23 B. Demirdjian, D. Ferry, J. Suzanne, O. B. Popovicheva, N. M. Persiantseva and N. K. Shonija, *J. Atmos. Chem.*, 2007, **56**, 83–103.
24 T. C. Hansen, P. F. Henry, H. E. Fisher, J. Torregrossa and P. Convert, *Meas. Sci. Technol.*, 2008, **19**, 034001.
25 P. Bernier and S. Lefrant, *Carbon molecules and materials*, Taylor and Francis Group, 2002.
26 B. Warren and P. Bodenstein, *Acta Crystallogr.*, 1965, **18**, 282–286.
27 J.-B. Donnet, R. C. Bansal, M.-J. Wang, *Carbon black: science and technology*, CRC Press, 1993.
28 L. Alexander and H. Kluh, *J. Appl. Phys.*, 1950, **21**, 137–143.
29 V. Tishkova, *Combustion nanoparticles from aviation and shipping*, Lamber Academic Publishing GmbH, 2010, ISBN: 978-3-8433-7963-2.
30 U. Kircher, V. Scheer and R. Vogt, *J. Phys. Chem. A*, 2000, **104**, 8908–8915.
31 J. A. Jassim, H. P. Lu, A. R. Chughtai and D. M. Smith, *J. Appl. Spectrosc.*, 1985, **40**, 113–116.
32 A. P. Terzyk, *Colloids Surf., A*, 2001, **177**, 23–45.
33 P. Carrott, *Carbon*, 1992, **30**, 201–205.
34 M. C. Bellissent-Funel, R. SridiDorbez and L. Bosio, *J. Chem. Phys.*, 1996, **104**, 10023.
35 N. K. Shonija, O. B. Popovicheva, N. M. Persiantseva, A. M. Savel'ev and A. M. Starik, *J. Geophys. Res.*, 2007, **112**, D02208.
36 L. Bosio, G. P. Johari and J. Teixeira, *Phys. Rev. Lett.*, 1986, **56**(3), 460–463.
37 E. Lui, J. Dore, J. B. W. Webber, D. Khushalani, S. T. Jahnert, G. H. Findenegg and T. Hansen, *J. Phys.: Condens. Matter*, 2006, **18**, 10009–10028.
38 J. Dore, B. Webber, D. Montage, T. Hansen, *Novel approaches to the structure and dynamics of liquids: experiments, theories and simulations*, Kluwer Academic Publisher, 2004, ISBN 1-4020-1846-0.
39 S. E. Antony, T. Tisdale, R. S. Disselkamp, M. A. Tolbert and J. C. Wilson, *Geophys. Res. Lett.*, 1995, **22**(9), 1105–1108.
40 K. L. Carleton, D. M. Sonnenfroh, W. T. Rawlins, B. E. Wyslouzil and S. Arnold, *J. Geophys. Res.*, 1997, **102**(D5), 6025–6033.
41 M. L. Clapp, L. Niedzela, J. Richwine, T. Dransfield, R. E. Miller and D. R. Worsnop, *J. Geophys. Res.*, 1997, **102**(D7), 8899–8907.
42 M. Ettner, S. K. Mitra and S. Borrman, *Atmos. Chem. Phys.*, 2004, **4**, 1925–1932.
43 J. B. Webber, J. C. Dore, J. H. Strange, R. Anderson and B. Tohidi, *J. Phys.: Condens. Matter*, 2007, **19**, 415117.
44 D. J. Cziczo, K. D. Froyd, S. J. Gallavardin, O. Moehler, S. Benz, H. Saathoff and D. M. Murphy, *Environ. Res. Lett.*, 2009, **4**, 044013.